

An Efficient Lorentz Equivariant Graph Neural Network for Jet Tagging

Shiqi Gong^{a,1} Qi Meng^b Jue Zhang^b Huilin Qu^c Congqiao Li^d Sitian Qian^d Weitao Du^a Zhi-Ming Ma^a Tie-Yan Liu^b

^a*Academy of Mathematics and Systems Science, Chinese Academy of Sciences, Zhongguancun East Road, Beijing 100190, China*

^b*Microsoft Research Asia, Danling Street, Beijing 100080, China*

^c*CERN, EP Department, CH-1211 Geneva 23, Switzerland*

^d*Department of Physics, Peking University, Chengfu Road, Beijing 100871, China*

E-mail: gongshiqi15@mails.ucas.ac.cn, meq@microsoft.com, tyliu@microsoft.com

ABSTRACT: Machine learning methods especially deep learning have become popular on jet representation in particle physics. Most of these methods focus on the handcrafted feature design or tuning the structure of existing black-box deep neural networks, while they ignore the Lorentz group equivariance, a fundamental space-time symmetry in the law for jet production. Inspired by the spirit that new physics insights may emerge more easily with the inclusion of underlying symmetry, we propose a new design of symmetry-preserving deep learning model named LorentzNet for jet tagging in this paper. Specifically, LorentzNet updates the geometric tensors via the Minkowski dot product attention, which aggregates the tensors with embedding of the pairwise Minkowski dot product as the weights. The construction of LorentzNet is guided by the universal approximation theory on Lorentz equivariant mapping which ensures the equivariance and the universality of the LorentzNet. Experiments on two representative jet tagging datasets show that LorentzNet can achieve the best tagging performance compared with the baselines (e.g., ParticleNet) on both clean and Lorentz rotated test data. Even with 0.5% fraction of training samples, LorentzNet still achieves competitive performance, which shows the benefit of the inductive bias brought by the Lorentz group symmetry.

¹This work was done when the first author was visiting Microsoft Research Asia.

Contents

1	Introduction	1
2	Preliminary	3
2.1	Notations	3
2.2	Theory of the Lorentz Group	3
2.3	Graph neural network for particle cloud	4
3	Network Architecture	5
3.1	LorentzNet	5
3.2	Theoretical Analysis	7
3.3	Implementation Details	8
4	Experiment	8
4.1	Datasets	8
4.2	Baselines and Tagging Performance	9
4.3	Sample Efficiency	11
4.4	Equivariance test	12
4.5	Ablation study	12
4.6	Computational cost	13
5	Conclusion	14
A	Details about LGN	15
B	Relation with EGNN	16

1 Introduction

Recently, machine learning methods especially deep learning has been widely adopted to a variety of problems in collider physics. Jet tagging is one of the most popular applications. Jets are collimated sprays of particles produced from energetic partons and jet tagging is to identify which type of elementary particle initiates the jet. Based on the theory and phenomenology in jet physics, many expert-designed high-level jet substructure observables are constructed for jet tagging [1, 2]. Compared with classic QCD based tagging methods, the machine learning based methods leverage the fine resolution of modern detectors through their ability to automatically construct powerful discrimination variables from low-level inputs, and they achieve very promising performance on jet tagging.

By choosing a suitable representation for jets, existing deep learning models can be directly applied to the task of jet tagging. For example, multilayer perceptrons (MLPs) can

be trained on lists of jets’ constituent particle momenta [3]; convolutional neural networks (CNNs) can be trained on jet images [4, 5, 5, 6]; 1D CNN and physics-oriented neural networks [7] are trained by viewing the jet as a collection of its particles; graph neural networks (GNNs) can be trained on an unordered set of particles viewed as a particle cloud [8–10]. These methods have led to substantial improvements in the performances of traditional taggers. However, few of these deep learning models are with particular regards to the fundamental symmetry in the law for jet production—although many models preprocess the jets in their representation to eliminate some arbitrariness in the space-time location of a jet (e.g., on the Lorentz boosts in the z -axis or the rotation on the x - y plane), few of them respect the Lorentz symmetry in the full space-time space intrinsic to the jet physics.

Symmetries have been shown to play a central role in many areas of physics. For example, the basic principle of special relativity is that all laws of physics appear equivalent to observers in all inertial frames. This fundamental symmetry is described by the Lorentz group in math. Therefore, the basic law under the production of jets and the physical quantities regarding the jet physics, such as the 4-momentum vector of a jet constituent, satisfy the Lorentz group symmetry. That means if one rotates the spatial-time inertial frame of the observer by the Lorentz transformation, the basic physical quantities for the jets such as the 4-momenta of the particles are rotated accordingly. This property is called equivariance to the Lorentz group. Intuitively, the group equivariance indicates a kind of linearity of the physical quantities with respect to the group representations. However, the features learned by many existing deep learning models can not ensure that their output representations satisfy the Lorentz group symmetry because the highly non-linear activation functions are applied freely to the input. Besides these models without symmetry, LoLa [7] and LBN [11] propose methods to improve the jet tagging performance by exploiting the underlying Lorentz symmetry of jets to some extent, e.g., these methods explore new types of layers or new particle features relevant to the Lorentz boost, but cannot guarantee the Lorentz equivariance property for the entire model. In [12], LGN - a Lorentz equivariant neural network architecture which is stacked by tensor products of representations of the Lorentz group is proposed. However, due to the explicit reliance on the high-order tensors in hidden layers, it is computationally expensive.

In this paper, we propose a new design of symmetry-preserving deep learning models for jet tagging. Using the particle cloud representation of the jets, we propose LorentzNet, which directly scalarizes the input tensors to realize Lorentz group symmetry. Specifically, we design Minkowski dot product attention, which aggregates the tensors with weights learned from scalars of the geometric tensors under the Minkowski metric. The scalars are fed into the deep neural networks to ensure the underlying weights can be well approximated. The construction of LorentzNet is guided by the universal approximation theory on Lorentz equivariant mapping which ensures the equivariance and the universality of the LorentzNet. Compared to LGN, LorentzNet does not require computationally expensive high-order tensors in hidden layers to ensure expressiveness, and it is more computationally efficient in terms of both training and inference.

Experiments on two representative jet tagging datasets show that LorentzNet can

achieve the best tagging performance compared with the baselines (e.g., ParticleNet). Even with 0.5% fraction of training samples on top tagging dataset, LorentzNet still achieves competitive performance, which clearly shows the benefit of the inductive bias brought by the Lorentz group symmetry on sample efficiency. Compared with the LGN, LorentzNet is more efficient and performs much better, which indicates a better tradeoff between the expressiveness and efficiency.

The rest of this paper is organized as follows. Sec. 2 reviews the theory of the Lorentz group symmetry. Sec. 3 introduces the architecture of LorentzNet. Sec. 4 details the experiments carried out on two jet tagging benchmarks to show the effectiveness of LorentzNet. Sec. 5 serves as the conclusion.

2 Preliminary

In this section, we introduce the foundation of the Lorentz group and describe the graph neural network for modelling particle clouds.

2.1 Notations

Following the jet representation in [8], we regard the particle sequence as a point cloud, which is an unordered, permutation invariant set of particles. Let $X = (x_1, \dots, x_N) \in \mathbb{R}^{N \times 4}$ denote the point clouds living in \mathbb{R}^4 and N denotes the number of particles in a jet. Note that the number of particles for jets may be different. $\langle \cdot, \cdot \rangle$ and $\| \cdot \|$ denote the Minkowski inner product and Minkowski norm. \oplus denotes the direct sum and \otimes denotes the tensor product. $[N]$ denotes the set $\{1, 2, \dots, N\}$.

2.2 Theory of the Lorentz Group

Minkowski metric. Consider the 4-dimensional space-time \mathbb{R}^4 with basis $\{e_i\}_{i=0}^3$. We define a bilinear form $\eta : \mathbb{R}^4 \times \mathbb{R}^4 \rightarrow \mathbb{R}$ as follows. Let $u, v \in \mathbb{R}^4$, we set $\eta(u, v) = u^T J v$ where $J = \text{diag}(1, -1, -1, -1)$ is the Minkowski metric. The inner product under this Minkowski metric for two vectors (t, x, y, z) and (t', x', y', z') are defined as $(t, x, y, z) \cdot (t', x', y', z') = tt' - xx' - yy' - zz'$. The Minkowski norm of a vector (t, x, y, z) is defined to be $\|v\| = \sqrt{|t^2 - x^2 - y^2 - z^2|}$.

Lorentz transformation. The Lorentz group is defined to be the set of all matrices that preserve the bilinear form η . Restricting the inertial frames to be positively oriented and positively time-oriented, we obtain proper orthochronous Lorentz group, denoted as $SO(1, 3)^+$. The 3d spatial rotation group $SO(3)$ is a subgroup of $SO(1, 3)^+$. Additionally, the Lorentz boost is also included. Given two inertial frames $\{e_i\}_{i=0}^3$ and $\{e'_i\}_{i=0}^3$, the relative velocity vector β and the boost factor γ are defined by $e'_0 = \gamma e_0 + \sum_{i=1}^3 \gamma \beta_i e_i$ where $\gamma = (1 - \beta^2)^{-1/2}$.

If we perform Lorentz boost along the x-spatial axis, then the Lorentz transformation between these two frames is the matrix

$$Q = \begin{pmatrix} \gamma & -\gamma\beta & 0 & 0 \\ -\gamma\beta & \gamma & 0 & 0 \\ 0 & 0 & 1 & 0 \\ 0 & 0 & 0 & 1 \end{pmatrix}.$$

Lorentz group equivariance. Let $T_g : X \rightarrow X$ be a set of Lorentz transformations on X for the Lorentz group $g \in G$. We say a function $\phi : X \rightarrow Y$ is equivariant to g if there exists an equivalent transformation on its output space $S_g : Y \rightarrow Y$ such that:

$$\phi(T_g(x)) = S_g(\phi(x)). \quad (2.1)$$

In this work, we only consider the case that the type of the output is scalar or vector. Therefore, we explore the following equivariance on a set of particles $X \in \mathbb{R}^{N \times 4}$. Let Q be the Lorentz transformation, the Lorentz equivariance of $\phi(\cdot)$ means:

$$Q\phi(x) = \phi(Qx), \quad \text{for } \phi(x) \in \mathbb{R}^4; \quad (2.2)$$

$$\phi(x) = \phi(Qx), \quad \text{for } \phi(x) \in \mathbb{R}. \quad (2.3)$$

Note that when the output is a scalar, the group equivariance equals to the group invariance.

2.3 Graph neural network for particle cloud

A jet can be denoted as a graph when we regard the constituent particles as nodes. For each particle, we use its 4-momentum vector (E, p_x, p_y, p_z) as the coordinate of a node in Minkowski space, and the scalars, such as mass, charge and particle identity information, to be node attributes. We index the particles in a jet as v_i and v_i contains essential features for tagging, which is denoted as $v_i = x_i \oplus s_i$ where $x_i = (E^i, p_x^i, p_y^i, p_z^i)$ denotes the 4-momentum vector and $s_i = (s_1^i, s_2^i, \dots, s_\alpha^i)$ denotes the sets of scalars. The graph can be denoted as $G = (V, E)$ where V is the set of nodes and E is the set of edges. The edges characterize the message passing between two particles, hence the interaction of two individual sets of particle-wise features. If there's no such interaction, there is no edge between the two particles. Here, we regard the graph as a fully connected undirected graph as we do not assume that we have any prior on the interactions among these particles.

Graph neural networks are natural to learn representations for graph structured data [13]. Given a graph $G = (V, E)$, the message passes on the graph usually in the following way [14]:

$$s_i^{l+1} = \sum_{j \in N(i)} M_l(h_i^l, h_j^l, e_{ij}); \quad (2.4)$$

$$h_i^{l+1} = U_l(h_i^l, s_i^{l+1}); \quad (2.5)$$

where $h_i^0 = v_i$, e_{ij} are the edge features, $N(i)$ is the set of neighbors of the node i and M_l, U_l are neural networks. For a classification problem, the output \hat{y} can be obtained by operating the softmax operator to $\{h_i^L; i \in [N]\}$.

Directly applying the message passing to the jet can not ensure the Lorentz group equivariance because the non-linear neural networks are applied directly to the whole input features and ignore its intrinsic structure. There are some variants of message passing designed to satisfy continuous group symmetry. A common way is to project the inputs to the basis of irreducible representations of the corresponding group, e.g., the LGN [12] which satisfies the Lorentz group equivariance. To ensure the universality, high order of the tensors should be realized by LGN, which brings high computational cost. (See detailed discussions in Appendix A).

In the next section, we will introduce the architecture of LorentzNet which is built upon a universal approximation theorem of Lorentz equivariant function and does not require computationally expensive higher-order representations.

3 Network Architecture

In this section, we illustrate the architecture of LorentzNet. The construction of the LorentzNet is based on the following universal approximation theorem for the Lorentz group equivariant continuous function.

Proposition 3.1. [15] *A continuous function $\phi : (\mathbb{R}^{N \times 4}) \rightarrow \mathbb{R}^4$ is Lorentz-equivariant if and only if*

$$\phi(x_1, x_2, \dots, x_N) = \sum_{i=1}^N g_i(\langle x_i, x_j \rangle_{i,j=1}^N) x_i, \quad (3.1)$$

where g_i are continuous Lorentz-invariant scalar functions, and $\langle \cdot, \cdot \rangle$ is the Minkowski inner product.

Proposition 3.1 provides a way to construct Lorentz group equivariant mapping with no need to calculate the high-order tensors. Instead, a Lorentz group equivariant continuous mapping can be constructed by the attention on x_i with encoding the Minkowski dot products of x_i with its neighbours. This motivates us to design the Minkowski dot product attention in LorentzNet, which will be introduced in the next section.

3.1 LorentzNet

We introduce the blocks in LorentzNet. As described in Fig. 1, LorentzNet is mainly constructed by the stack of Lorentz Group Equivariant block (LGEB) along with encoder and decoder layers.

Input layer. The inputs into the network are 4-momenta of particles from a collision event, and may include scalars associated with them (such as label, charge, etc.). That is, the input is a set of vectors $v_i = x_i \oplus s_i$ where $x_i = (E^i, p_x^i, p_y^i, p_z^i)$ denotes the 4-momentum vector and $s_i = (s_1^i, s_2^i, \dots, s_\alpha^i)$ is the collection of scalars. In the experiments in this paper, the scalars include the mass of the particle (i.e., $(E^i)^2 - (p_x^i)^2 - (p_y^i)^2 - (p_z^i)^2$) and a label distinguishing observed decay products from the collider beams, or particle identification (PID) information directly if it is available.

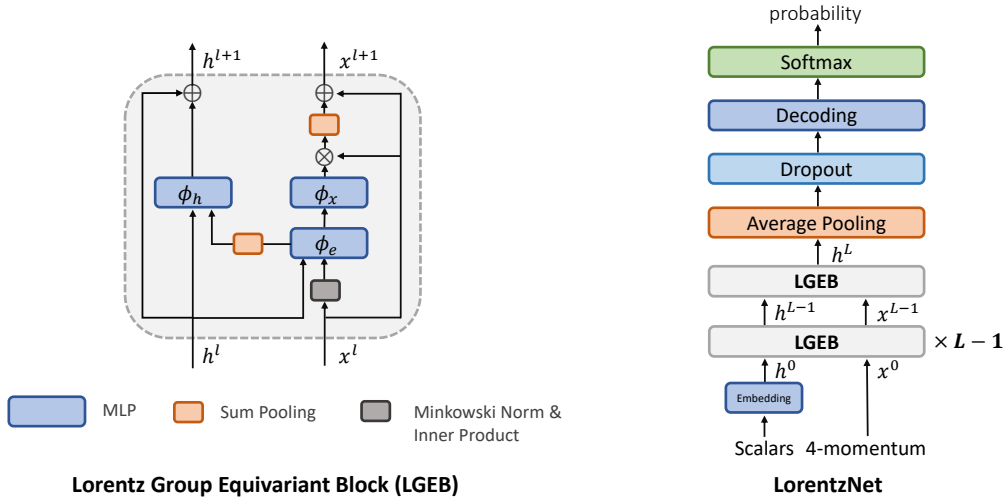


Figure 1. (left): The structure of the Lorentz Group Equivariant Block (LGEB). (right): The network architecture of the LorentzNet.

Lorentz Group Equivariant Block. We use $h^l = (h_1^l, h_2^l, \dots, h_n^l)$ to denote the node embedding scalars, and $x^l = (x_1^l, x_2^l, \dots, x_n^l)$ to denote the coordinate embedding vectors in the l -th LGEB layer. When $l = 0$, x^0 equals the input of the 4-momenta and $h_i^0 = s_i$ denotes the input of the scalar variables. LGEB aims to learn deeper embeddings h^{l+1}, x^{l+1} via current h^l, x^l . Motivated by Equation (3.1), the message passing of LorentzNet is written as follows. We use m_{ij} to denote the edge message between particle i and j , and it encodes the scalar information of the particle i and j , i.e.,

$$m_{ij}^l = \phi_e \left(h_i^l, h_j^l, \psi(\|x_i^l - x_j^l\|^2), \psi(\langle x_i^l, x_j^l \rangle) \right), \quad (3.2)$$

where $\phi_e(\cdot)$ is a neural network and $\psi(\cdot) = \text{sgn}(\cdot) \log(|\cdot| + 1)$ in Equation (3.2) is a normalizing function to make the heavy tailed distributed quantities centralized for ease of optimization. Except for the embedding of the scalar features h_i^l and h_j^l , according to Proposition 3.1, the input of the neural network contains the Minkowski dot product $\langle x_i, x_j \rangle$. The $\|x_i^l - x_j^l\|^2$ is also included because the interaction between particles relies on this term and we include it as a prior feature for ease of learning.

According to Equation (3.1), we design *Minkowski dot product attention* as

$$x_i^{l+1} = x_i^l + c \sum_{j \neq i} \phi_x(m_{ij}^l) \cdot x_j^l \quad (3.3)$$

where $\phi_x(\cdot) \in \mathbb{R}$ is a scalar function modeled by neural networks. To ensure the equivariance, we can not arbitrarily apply the normalization trick to control the scale of x_i^{l+1} . Therefore, we introduce the hyperparameter c to control the forward stability together with the shortcut connection. This step captures the interactions of the i -th particle with other particles via the ensemble of the 4-momenta of all particles. Unlike most of the symmetry-preserving neural networks such as LGN and EGNN [16] (for $E(n)$ equivariance)¹ which

¹The relation with EGNN is discussed in the Appendix.

only include the radial distance $\|x_i - x_j\|^2$ as the only scalars extracted from the vector representation, we include the dot product $\langle x_i, x_j \rangle$ in m_{ij} to recover the information of angles according to Equation (3.1) which can not be captured by the radial distance.

The scalar features for particle i is forward as

$$h_i^{l+1} = h_i^l + \phi_h(h_i^l, \sum_{j \neq i} w_{ij} m_{ij}^l), \quad (3.4)$$

where $\phi_h(\cdot)$ is also modeled by neural networks whose output dimension equals the dimension of h_i^{l+1} . For efficient computation, we operate summation $\sum_{j \neq i} w_{ij} m_{ij}^l$ to aggregate m_{ij}^l . This can both ensure the permutation invariance but also ease the implementation for jets with different number of particles. This operation is also widely adopted in other types of graph neural networks [14, 16].

Decoding layer. After stacks of LGEB for L layers, we decode the node embedding $h^L = (h_1^L, \dots, h_N^L)$. Note that the information of x^{L-1} has been included in h^L through the m_{ij}^{L-1} . Therefore, to avoid redundant information, we only decode h^L . First we use average pooling to get

$$h^{av} = \sum_i h_i^L. \quad (3.5)$$

A subsequent dropout layer is applied to h^{av} to prevent overfitting. A decoding block with two fully connected layers, followed by a softmax function, is used to generate the output for the binary classification task.

3.2 Theoretical Analysis

In this section, we analyze the Lorentz group equivariance of LorentzNet.

Proposition 3.2. *The coordinate embedding $x^l = (x_1^l, x_2^l, \dots, x_N^l)$ are Lorentz group equivariant and the node embedding $h^l = (h_1^l, \dots, h_N^l)$ are Lorentz group invariant.*

Proof: We denote Q as the Lorentz transformation. If m_{ij}^l are invariant under Q for all i, j, l , x_i^{l+1} will be Lorentz group equivariant because

$$\begin{aligned} Qx_i^{l+1} &= Q(x_i^l + c \sum_{j \neq i} (x_i^l - x_j^l) \phi_x(m_{ij}^l)) \\ &= Qx_i^l + c \sum_{j \neq i} (Qx_i^l - Qx_j^l) \phi_x(m_{ij}^l). \end{aligned}$$

Then we illustrate the invariance of m_{ij}^l . We start from the input. Since the 4-momentum vector are Lorentz group equivariant, we have $\|x_i^0 - x_j^0\|^2 = \|Qx_i^0 - Qx_j^0\|^2$ because the determinant of Q equals 1, and similar for $\langle x_i^0, x_j^0 \rangle$. Therefore, the input of ϕ_e are invariant variables under transformation Q and then m_{ij}^0 are invariant. Recursively using the invariance of m_{ij}^l and the equivariance of x_i^l , we can get the conclusion. \square

As for the expressiveness of the LGEB structure, we have the following discussions. Because h_i is a function of the aggregation of m_{ij} , it contains the information of all the

Minkowski dot products of the particle pairs. Therefore, the weights in Minkowski dot product attention $\phi_x(\cdot)$ at l -th layer ($l > 1$) contain all the Minkowski dot products of the particle pairs. According to Proposition 3.1, the input information of the attention factor is complete for expressiveness.

3.3 Implementation Details

The LorentzNet architecture used in this paper is shown in Fig. 1. It consists of 6 Lorentz group equivariant blocks ($L = 6$). The scalar embedding is implemented as one fully connected layer which maps the scalars to latent space of width 72, i.e., $\text{LINEAR}(scalar_dim, 72)$. ϕ_x, ϕ_e, ϕ_h are all implemented as $\text{LINEAR}(72, 72) \rightarrow \text{RELU} \rightarrow \text{BATCHNORM1D}(72) \rightarrow \text{LINEAR}(72, 72)$. The decoding layers are $\text{LINEAR}(72, 72) \rightarrow \text{RELU} \rightarrow \text{LINEAR}(72, 2)$. The dropout rate here is 0.2. The hyperparameter c in Equation (3.3) are chosen to be 5×10^{-3} and 1×10^{-3} for the top tagging and the quark-gluon tagging task respectively to achieve the best performances.

The networks are implemented with PyTorch and the training is performed on a cluster with four Nvidia Tesla V100 GPUs. A batch size of 32 is used on each single GPU for LorentzNet architecture. The ADAMW [17] optimizer, with a weight decay of 0.01, is used to minimize the cross entropy loss. The LorentzNet is trained for 35 epochs in total. Firstly a linear warm-up period of 4 epochs is applied to reach the initial learning rate 1×10^{-3} . Then a COSINEANNEALINGWARMRESTARTS [18] learning rate schedule with $T_0 = 4$, $T_{mult} = 2$ is adopted for next 28 epochs. Finally an exponential learning rate decay with $\gamma = 0.5$ is used for the last 3 epochs. We test the model on the validation dataset at the end of each training epoch, and the model with the highest validation accuracy is saved as our best model for the final test.

4 Experiment

The performance of the LorentzNet architecture is evaluated on two representative jet tagging tasks: top tagging and quark-gluon tagging. In this section, we show the benchmark results.

4.1 Datasets

Top tagging. We first evaluate LorentzNet on top tagging classification experiments with the publicly available reference dataset [19]. This dataset contains 1.2M training entries, 400k validation entries and 400k testing entries. Each of these entries represents a single jet whose origin is either an energetic top quark, a light quark, or a gluon. The events are produced using the PYTHIA8 Monte Carlo event generator. The ATLAS detector response is modelled with the DELPHES software package.

The jets in the reference dataset are clustered using the anti- k_T algorithm, with a radius of $R = 0.8$. For each jet, the 4-momenta are saved in Cartesian coordinates (E, p_x, p_y, p_z) for up to 200 constituent particles selected by the highest transverse momentum where the colliding particle beams are aligned along the z -axis. Each jet contains an average of 50 particles, and events with less than 200 are zero-padded.

Quark-gluon tagging. The second dataset is for quark-gluon tagging, i.e., discriminating jets initiated by quarks and by gluons. The signal (quark) and background (gluon) jets are generated with `PYTHIA8` using the $Z(\rightarrow \nu\nu) + (u, d, s)$ and $Z(\rightarrow \nu\nu) + g$ processes, respectively. No detector simulation is performed. The final state non-neutrino particles are clustered into jets using the anti- k_T algorithm with $R = 0.4$. This dataset consists of 2 million jets in total, half signal and half background. We follow the setting in [8] to split 1.6M/200K/200K for training, validation and testing.

One difference of the quark-gluon tagging dataset is that it includes not only the 4-momentum vector, but also the type of each particle (i.e., electron, photon, pion, etc.). We use the one-hot encoding of the type of each particle as input scalars into the LorentzNet. We include this task to test the performance of LorentzNet under this different type of input features.

4.2 Baselines and Tagging Performance

We compare the performance of LorentzNet with six baseline models: ResNeXt-50 [20], P-CNN [21], PFN [22], ParticleNet [8], EGNN [16] and LGN [12]. The tagging accuracy of these six models except EGNN has been reported in [8] and [12]. In this paper, we also investigate their robustness under Lorentz transformation and the computational cost. For self-contained, we briefly introduce them here. The ResNeXt-50 model is a 50 layer convolutional neural network with skip connections for image classification. Representing jets as images, we can apply ResNeXt-50 to jet tagging. The P-CNN is a 14-layer 1D CNN using particle sequences as inputs. The P-CNN architecture was proposed in the CMS particle-based DNN boosted jet tagger and showed significant improvement in performance compared to a traditional tagger using boosted decision trees and jet-level observables. The Particle Flow Network (PFN) and the ParticleNet also treats a jet as an unordered set of particles. The PFN is based on the Deep Sets framework. The ParticleNet is based on Dynamic Graph Convolutional Neural Network with carefully design on the EdgeConv operation. We also include EGNN as a representative symmetry-preserving model as our baseline which is $E(4)$ equivariant. It is different from LorentzNet that EGNN uses metrics in Euclidean space instead of Minkowski space. We compare LorentzNet with EGNN to show the necessity of Lorentz group symmetry. For a fair comparison, we set the number of parameters of EGNN in the same order with LorentzNet.

For ResNeXt, P-CNN, PFN, and ParticleNet, we follow the implementation in [8]. For LGN, we follow the implementation in [12] on top tagging. For the quark-gluon dataset, the implementation details are reported in Appendix A.

Tagging performance. The results for the top tagging dataset and quark-gluon dataset are summarized in Table 1 and Table 2, respectively. We adopt the widely used measures to evaluate the performance of the LorentzNet model including accuracy, the Area Under the ROC Curve (AUC)², the background rejection $1/\varepsilon_B$ at the signal efficiency of $\varepsilon_S = 0.3$ and

²ROC curve is a plot of the true positive rate (Sensitivity) in the function of the false positive rate (100-Specificity) for different cut-off points of a parameter. Each point on the ROC curve represents a sensitivity/specificity pair corresponding to a particular decision threshold. The Area Under the ROC

Model	Accuracy	AUC	$1/\varepsilon_B$ ($\varepsilon_S = 0.5$)	$1/\varepsilon_B$ ($\varepsilon_S = 0.3$)
ResNeXt	0.936	0.9837	302 ± 5	1147 ± 58
P-CNN	0.930	0.9803	201 ± 4	759 ± 24
PFN	0.932	0.9819	247 ± 3	888 ± 17
ParticleNet	0.940	0.9858	397 ± 7	1615 ± 93
EGNN	0.922	0.9760	148 ± 8	540 ± 49
LGN	0.929	0.9640	124 ± 20	435 ± 95
LorentzNet	0.942	0.9868	498 ± 18	2195 ± 173

Table 1. Performance comparison between LorentzNet and other representative algorithms on top tagging dataset. The results for LorentzNet and EGNN are averaged on 6 runs. The results for other baselines are referred to [8, 12, 22].

Model	Accuracy	AUC	$1/\varepsilon_B$ ($\varepsilon_S = 0.5$)	$1/\varepsilon_B$ ($\varepsilon_S = 0.3$)
ResNeXt	0.821	0.8960	30.9	80.8
P-CNN	0.827	0.9002	34.7	91.0
PFN	–	0.9005	34.7 ± 0.4	–
ParticleNet	0.840	0.9116	39.8 ± 0.2	98.6 ± 1.3
EGNN	0.803	0.8806	26.3 ± 0.3	76.6 ± 0.5
LGN	0.803	0.8141	8.30	15.2
LorentzNet	0.844	0.9156	42.4 ± 0.4	110.2 ± 1.3

Table 2. Performance comparison between LorentzNet and other representative algorithms on quark-gluon tagging dataset. The results for LorentzNet, EGNN and LGN are averaged on 6 runs. The results for other baselines are referred to [8, 22].

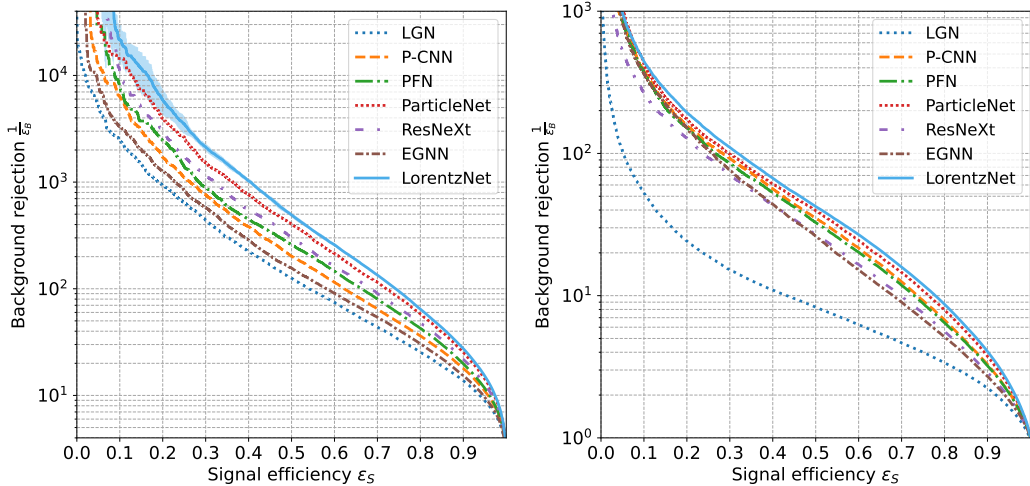


Figure 2. A comparison of ROC curves between LorentzNet and other algorithms on top tagging dataset (left) and quark-gluon dataset (right).

0.5 (ε_B , ε_S are also known as the false positive and the true positive rates, respectively), and the number of trainable parameters. Especially, the background rejection metric is widely adopted to select the best jet tagging algorithm as it is directly related to the expected contribution of the background [8, 12, 22].

From Table 1 and Table 2, we conclude that LorentzNet achieves the state-of-the-art performance on both the top tagging dataset and the quark-gluon in terms of the accuracy, AUC, and background rejection at $\varepsilon_S = 0.3, 0.5$. The results verify the effectiveness of LorentzNet compared with the baselines. Fig. 2 shows the background rejection at a fine-grained signal efficiency. The ROC curves of LorentzNet achieve the highest score at all the selected signal efficiency compared to the baselines. Especially, LorentzNet shows superiority compared to the LGN. Especially, it achieves 4 or 5 times improvement on the background rejection. The results verify our discussions in Section 3.2.

Training Fraction	Model	Accuracy	AUC	$1/\varepsilon_B$ ($\varepsilon_S = 0.5$)	$1/\varepsilon_B$ ($\varepsilon_S = 0.3$)
0.5%	ParticleNet	0.913	0.9687	77 ± 4	199 ± 14
	LorentzNet	0.929	0.9793	176 ± 14	562 ± 72
1%	ParticleNet	0.919	0.9734	103 ± 5	287 ± 19
	LorentzNet	0.932	0.9812	209 ± 5	697 ± 58
5%	ParticleNet	0.931	0.9807	195 ± 4	609 ± 35
	LorentzNet	0.937	0.9839	293 ± 12	1108 ± 84

Table 3. Performance comparison between LorentzNet and ParticleNet on top tagging dataset by a fraction of training data. The results are all averaged on 6 runs.

4.3 Sample Efficiency

The benefit of the preservation of Lorentz group symmetry in jet tagging has not been studied in literature. In theory, the Lorentz group symmetry injects inductive bias into the deep learning model which restricts the function class of the hypothesis space. The inductive bias can help to boost the generalization and improve the sample efficiency. As the improvement on the generalization performance (i.e., the tagging accuracy) has been shown in the previous section, we show the robustness of LorentzNet trained on smaller training data to verify the sample efficiency of LorentzNet in this part.

We choose the best performed architecture among the models with and without fully Lorentz group symmetry (i.e., the LorentzNet and the ParticleNet) to compare. The inductive bias in ParticleNet is a subgroup symmetry of Lorentz group, which only consider the Lorentz boosts in the z -axis and the rotation on the $x - y$ plane, while LorentzNet is symmetric to Lorentz group. We random select 5%, 1%, and 0.5% fraction of training data to train the LorentzNet and ParticleNet on top tagging dataset, and we test the performance of them on the same test data with size 400k. The training strategy keeps the same with the experiments on the full training data. The results are reported in Table 3. The gap of

curve (AUC) is a measure of how well a parameter can distinguish between two diagnostic groups.

the tagging accuracy and AUC between LorentzNet and ParticleNet becomes larger as the number of the training data becomes smaller. The results clearly show the benefit of the preservation of Lorentz group symmetry in jet tagging.

4.4 Equivariance test

Another advantage of symmetry-preserving deep learning models is their robustness under Lorentz transformation. To verify it, we rotate the test data by Lorentz transformation with different scales of β along the x axis, i.e., the value of (E, p_x) in the 4-momentum vector will be rotated. As β becomes larger, the difference between the distributions of training and test data will become larger. We test the model trained on the original training data on the rotated test data and the tagging accuracy on the rotated test data is reported in Fig. 3. The horizontal axis of Fig. 3 shows the value of β and the vertical axis shows the tagging accuracy on the top tagging dataset under Lorentz transformation with corresponding β . Fig. 3 shows that the test accuracy of LorentzNet and LGN on the test data after Lorentz transformation is robust in a large range of β , while the test accuracy of other non-equivariant models will drop as β becomes larger. According to special relativity, the fundamental quantities to clarify the particles will not be changed. The results show that only the Lorentz group equivariant models LorentzNet and LGN can capture this symmetry. Even compared with LGN, LorentzNet is more stable when β approaches 1 and the instability of LGN is caused by the rounding errors in float arithmetic as described in its original paper [12].

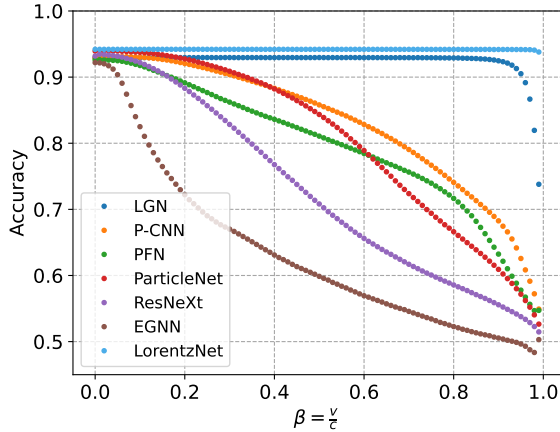


Figure 3. Equivariant test under Lorentz boosts on top tagging dataset.

4.5 Ablation study

In this section, we report the results of the ablation study to further demonstrate the effectiveness of the components in LorentzNet. To show the effectiveness of keeping the Lorentz group equivariance, we directly use x_i^l, x_j^l as inputs of the ϕ_e to break the Lorentz group equivariance because x_i^l, x_j^l are not Lorentz group invariant variables, i.e., the Equation

Model	Equivariance	Accuracy	AUC	$1/\varepsilon_B$ ($\varepsilon_S = 0.5$)	$1/\varepsilon_B$ ($\varepsilon_S = 0.3$)
LorentzNet (w/o)	✗	0.934	0.9832	290 ± 30	1105 ± 59
LorentzNet	✓	0.942	0.9868	498 ± 18	2195 ± 173

Table 4. Performance comparison between LorentzNet and corresponding non-equivariant version on top tagging dataset. Both of the results are averaged on 6 runs.

Model	Equivariance	Time on CPU (ms/batch)	Time on GPU (ms/batch)	#Params
ResNeXt	✗	5.5	0.34	1.46M
P-CNN	✗	0.6	0.11	348k
PFN	✗	0.6	0.12	82k
ParticleNet	✗	11.0	0.19	366k
EGNN	E(4)	30.0	0.30	222k
LGN	SO ⁺ (1,3)	51.4	1.66	4.5k
LorentzNet	SO ⁺ (1,3)	32.9	0.34	224k

Table 5. Inference time of each model on both CPU and GPU along with their parameter numbers. Models are executed on a cluster with an Intel Xeon CPU E5-2698 v4 and an Nvidia Tesla V100 32GB. Both of the inference times are collected with a batch size of 100.

(3.2) is replaced by

$$m_{ij} = \phi_e(x_i^l, x_j^l, h_i^l, h_j^l), \quad (4.1)$$

We name this variant as LorentzNet without equivariance (abbreviated as LorentzNet (w/o)). We compare the performance of LorentzNet (w/o) with LorentzNet on the top tagging dataset. The hyperparameters of training LorentzNet (w/o) keep the same with LorentzNet and we train LorentzNet (w/o) till it converges. As shown in Table 4, LorentzNet (w/o) performs worse than LorentzNet, which shows the necessity of the Lorentz group equivariance on the tagging performance.

4.6 Computational cost

We report the inference time of LorentzNet and other baseline models. The inference time of each model on both CPU and GPU along with the number of their parameters are reported in Table 5. The number of trainable parameters of LorentzNet is in the same order with P-CNN, ParticleNet. Models are executed on a cluster with an Intel Xeon CPU E5-2698 v4 and an Nvidia Tesla V100 32GB GPU. Both of the inference times are collected with a batch size of 100. As shown in Table 5, the inference time on GPU of LorentzNet is slightly larger than P-CNN, PFN and particleNet and is comparable with ResNeXt. Especially, compared with LGN, the LorentzNet is almost 5 times faster on GPU, although the number of trainable parameters of LGN is much smaller. For the inference time on CPU, LorentzNet is also faster than LGN. Both results demonstrate the efficiency of LorentzNet. Since there’s no need to compute the high-order tensors for LorentzNet, it is

more efficient. The main computational cost of LorentzNet comes from its message passing on the fully connected graph. Its cost linearly depends on the number of particles in a jet. This cost can be reduced by clustering the nodes and we will explore it for future study.

5 Conclusion

We have presented the LorentzNet, a Lorentz group equivariant graph neural network for jet tagging. We showed that LorentzNet can achieve the best accuracy over all existing methods. Although we evaluate the effectiveness of LorentzNet for the jet tagging problem on two datasets, the whole model architecture may be applied to other tasks on jets, such as, regression - predicting the true jet mass/momentum; generation - simulating jet data, as well as the full collision event, classifying signal vs background processes, pileup mitigation, etc. As ever-larger science and engineering datasets become available for particle physics, we hope that LorentzNet will help enable more accurate prediction as well as aid the discovery of interesting new phenomena.

Acknowledgments

We thank Wei Chen (MSRA) for her helpful discussions on symmetry-preserving deep learning models and support.

References

- [1] R. Kogler, B. Nachman, A. Schmidt, L. Asquith, E. Winkels, M. Campanelli et al., *Jet substructure at the large hadron collider*, *Reviews of Modern Physics* **91** (2019) 045003.
- [2] A.J. Larkoski, I. Moult and B. Nachman, *Jet substructure at the large hadron collider: a review of recent advances in theory and machine learning*, *Physics Reports* **841** (2020) 1.
- [3] J. Pearkes, W. Fedorko, A. Lister and C. Gay, *Jet constituents for deep neural network based top quark tagging*, *arXiv preprint arXiv:1704.02124* (2017) .
- [4] J. Cogan, M. Kagan, E. Strauss and A. Schwartzman, *Jet-images: computer vision inspired techniques for jet tagging*, *Journal of High Energy Physics* **2015** (2015) 1.
- [5] L. de Oliveira, M. Kagan, L. Mackey, B. Nachman and A. Schwartzman, *Jet-images—deep learning edition*, *Journal of High Energy Physics* **2016** (2016) 1.
- [6] P.T. Komiske, E.M. Metodiev and M.D. Schwartz, *Deep learning in color: towards automated quark/gluon jet discrimination*, *Journal of High Energy Physics* **2017** (2017) 1.
- [7] A. Butter, G. Kasieczka, T. Plehn and M. Russell, *Deep-learned top tagging with a lorentz layer*, *SciPost Phys* **5** (2018) 028.
- [8] H. Qu and L. Gouskos, *Jet tagging via particle clouds*, *Physical Review D* **101** (2020) 056019.
- [9] V. Mikuni and F. Canelli, *Abcnet: An attention-based method for particle tagging*, *The European Physical Journal Plus* **135** (2020) 1.
- [10] V. Mikuni and F. Canelli, *Point cloud transformers applied to collider physics*, *Machine Learning: Science and Technology* (2021) .

- [11] M. Erdmann, E. Geiser, Y. Rath and M. Rieger, *Lorentz Boost Networks: Autonomous Physics-Inspired Feature Engineering*, *JINST* **14** (2019) P06006 [[1812.09722](#)].
- [12] A. Bogatskiy, B. Anderson, J. Offermann, M. Roussi, D. Miller and R. Kondor, *Lorentz group equivariant neural network for particle physics*, in *International Conference on Machine Learning*, pp. 992–1002, PMLR, 2020.
- [13] F. Scarselli, M. Gori, A.C. Tsoi, M. Hagenbuchner and G. Monfardini, *The graph neural network model*, *IEEE transactions on neural networks* **20** (2008) 61.
- [14] J. Gilmer, S.S. Schoenholz, P.F. Riley, O. Vinyals and G.E. Dahl, *Neural message passing for quantum chemistry*, in *International conference on machine learning*, pp. 1263–1272, PMLR, 2017.
- [15] S. Villar, D. Hogg, K. Storey-Fisher, W. Yao and B. Blum-Smith, *Scalars are universal: Equivariant machine learning, structured like classical physics*, *Advances in Neural Information Processing Systems* **34** (2021) .
- [16] V.G. Satorras, E. Hoogeboom and M. Welling, *E (n) equivariant graph neural networks*, *arXiv preprint arXiv:2102.09844* (2021) .
- [17] I. Loshchilov and F. Hutter, *Decoupled weight decay regularization*, in *International Conference on Learning Representations*, 2018.
- [18] I. Loshchilov and F. Hutter, *Sgdr: Stochastic gradient descent with warm restarts*, *arXiv preprint arXiv:1608.03983* (2016) .
- [19] G. Kasieczka, T. Plehn, J. Thompson and M. Russel, *Top quark tagging reference dataset*, 2019.
- [20] S. Xie, R. Girshick, P. Dollár, Z. Tu and K. He, *Aggregated residual transformations for deep neural networks*, in *Proceedings of the IEEE conference on computer vision and pattern recognition*, pp. 1492–1500, 2017.
- [21] C. collaboration et al., *Boosted jet identification using particle candidates and deep neural networks*, *CMS Detector Performance Report CMS-DP-2017-049* (2017) .
- [22] P.T. Komiske, E.M. Metodiev and J. Thaler, *Energy flow networks: deep sets for particle jets*, *Journal of High Energy Physics* **2019** (2019) 1.
- [23] W. Du, H. Zhang, Y. Du, Q. Meng, W. Chen, B. Shao et al., *Equivariant vector field network for many-body system modeling*, *arXiv preprint arXiv:2110.14811* (2021) .

A Details about LGN

In this section, we first introduce the architecture of LGN and analyze its stability and computational efficiency.

The input of LGN is the same as LorentzNet. The node features h^{l+1} for LGN is obtained by

$$h_i^l \oplus CG(h_i^l \otimes h_i^l) \oplus CG\left(\sum_j \phi_x(\|x_i - x_j\|^2)(x_i - x_j) \otimes h_j^l\right), \quad (\text{A.1})$$

where $CG(\cdot \otimes \cdot)$ denotes the Clebsch-Gordan tensor product and $\phi_x(\cdot)$ denotes a neural network. The term h_i^l is the shortcut connection. The middle term reflects the self-interaction

and the last term reflects the interaction of the i 'th particle with other particles. A multi-layer perceptron layer will be added to operate on the scalar representations of the Lorentz group after the operating Equation (A.1). The Clebsch-Gordan tensor product projects tensors to different orders of an irreducible representation of the Lorentz group, i.e.,

$$e_{l,m}^{(k,n)} \rightarrow \sum H_{(k,n),l,m}^{(k_1,n_1),l_1,m_1;(k_2,n_2),l_2,m_2} e_{l_1,m_1}^{(k_1,n_1)} \otimes e_{l_2,m_2}^{(k_2,n_2)}, \quad (\text{A.2})$$

where $H_{(k,n),l,m}^{(k_1,n_1),l_1,m_1;(k_2,n_2),l_2,m_2}$ denotes the Clebsch-Gordan coefficient, $e_{(l,m)}^{(k,n)}$ denotes the canonical basis of the (k,n) -order irreducible representation of the Lorentz group where $l = |k - n|/2, \dots, (k + n)/2; m = -l, \dots, l$.

Ideally, the universal approximation of the LGN can be achieved if the order of tensors that LGN realized is sufficiently high. However, in practice, the order of tensors should be cutoff for efficient computation and there is no direct prior to determining this cutoff in many applications.

In terms of the computational efficiency, one problem is that the tensor product brings the computational cost to (Eq.(A.2)) compared with the simple dot product in LorentzNet. Another problem is that the tensor product operation is a weighted sum of products of the input features. Without normalization, the output of the network will be sensitive to the scale of the input, which leads to instability (e.g., value explosion or vanish) to both the forward and backward processes. To ensure stability, the input 4-momenta were scaled by a factor of 0.005 on top tagging dataset in the original paper [12]. The scaling factor is a hyper-parameter to tune for different datasets. However, there is no principle way designed for the scaling or normalization which can stabilize the training process and keep the Lorentz symmetry meanwhile. Therefore, compared with LGN, LorentzNet can achieve a better tradeoff between approximation ability and computational efficiency.

In the experiments of LGN on quark-gluon dataset, we follow its public code base in <https://github.com/fizisist/LorentzGroupNetwork>. The batch size is set to be 48 and we run 20 epochs in total. The wall block time of running one epoch of LGN is more than 10 times larger than other baseline models, which is also reported in its original paper [12] (e.g., 7.5 hours per epoch with batch size 8 on top tagging). The computational efficiency is a main bottleneck for further evaluation on LGN.

B Relation with EGNN

The message passing of LorentzNet is also inspired by EGNN, which is proposed to ensure $E(n)$ group equivariance. If the output is a scalar, the message passing of EGNN is written as:

$$m_{ij}^{l+1} = \phi_e(h_i^l, h_j^l, \|x_i - x_j\|_E); \quad (\text{B.1})$$

$$h_i^{l+1} = \phi_h(h_i^l, \sum_{j \neq i} m_{ij}^l), \quad (\text{B.2})$$

where $\|\cdot\|_E$ denotes the L^2 norm under Euclidean metric.

We discuss the difference between LorentzNet and EGNN. First, EGNN uses the Euclidean norm of the relative distance as the only scalar information of the vector. Since relative distance can not recover the information of the angles (i.e., the inner products), its expressiveness is arguable [23]. In the context of $E(n)$ equivariant, the inner product $\langle x_i, x_j \rangle$ can not be added because of the translation invariance. As we target Lorentz group symmetry, we can include the Minkowski inner product for information completeness. Second, EGNN does not include the coordinate update component for scalar prediction while LorentzNet includes the Minkowski dot product attention for expressiveness. For fair comparison in the experiments, we include the coordinate update step $x_i^{l+1} = x_i^l + \sum_{j \neq i} (x_j - x_i) \phi_x(m_{ij}^l)$ in EGNN to ensure the difference only caused by different groups.

In the experiments of EGNN on top and quark-gluon dataset, we follow its public code base in <https://github.com/vgsatorras/egnn>. We use a batch size of 128 in the training process for 35 epochs in total. The ADAMW [17] optimizer, with a weight decay of 0.01, is used to minimize the cross entropy loss. Firstly a linear warm-up period of 4 epochs is applied to reach the initial learning rate 1×10^{-3} . Then a COSINEANNEALINGWARM-RESTARTS [18] learning rate schedule with $T_0 = 4$, $T_{mult} = 2$ is adopted for next 28 epochs. Finally an exponential learning rate decay with $\gamma = 0.5$ is used for the last 3 epochs. We test the model on the validation dataset at the end of each training epoch, and the model with the highest validation accuracy is saved as our best model for the final test.